



LAWRENCE  
LIVERMORE  
NATIONAL  
LABORATORY

# Analytic Solution of the Envelope Equations for an Undepressed Matched Beam in a Quadrupole Doublet Channel

O. A. Anderson, L. L. LoDestro

May 1, 2009

PAC2009  
Vancouver, Canada  
May 4, 2009 through May 8, 2009

## **Disclaimer**

---

This document was prepared as an account of work sponsored by an agency of the United States government. Neither the United States government nor Lawrence Livermore National Security, LLC, nor any of their employees makes any warranty, expressed or implied, or assumes any legal liability or responsibility for the accuracy, completeness, or usefulness of any information, apparatus, product, or process disclosed, or represents that its use would not infringe privately owned rights. Reference herein to any specific commercial product, process, or service by trade name, trademark, manufacturer, or otherwise does not necessarily constitute or imply its endorsement, recommendation, or favoring by the United States government or Lawrence Livermore National Security, LLC. The views and opinions of authors expressed herein do not necessarily state or reflect those of the United States government or Lawrence Livermore National Security, LLC, and shall not be used for advertising or product endorsement purposes.

# ANALYTIC SOLUTION OF THE ENVELOPE EQUATIONS FOR AN UNDEPRESSED MATCHED BEAM IN A QUADRUPOLE DOUBLET CHANNEL \*

O. A. Anderson, LBNL, Berkeley, CA 94720, USA  
L. L. LoDestro, LLNL, Livermore, CA 94551, USA

## Abstract

In 1958, Courant and Snyder analyzed the problem of alternating-gradient beam transport and treated a model without focusing gaps or space charge. Recently we revisited their work and found the exact solution for matched-beam envelopes in a linear quadrupole lattice [O.A. Anderson and L.L. LoDestro, Phys. Rev. ST Accel. Beams, 2009]. We extend that work here to include the effect of asymmetric drift spaces. We derive the solution and show exact envelopes for the first two solution bands and the peak envelope excursions as a function of the phase advance  $\sigma$  up to  $360^\circ$ . In the second stable band, decreased occupancy requires higher focusing strength. For symmetric gaps, this accentuates the remarkable compression effect predicted for the FD (gapless) model.

## INTRODUCTION

In their classic paper, Courant and Snyder [1] studied the beam-envelope dynamics of a circular machine with negligible space charge, piecewise constant focusing, and no drift spaces (focusing gaps); they used an expansion in focusing strength to obtain an approximate solution for the matched envelope. The same case, but for a straight machine, was recently analyzed and an exact solution was obtained [2]. In the present paper we extend that recent analysis to include asymmetric focusing gaps, still assuming negligible space charge. Of course, particular cases with asymmetric gaps have long been studied via computer simulations; numerical examples with space charge are found in Refs. [3] and [4]. The motivations for finding the exact analytic envelope solution are: (1) performing parametric studies and studying the properties of the solutions such as extrema, limits, etc.; (2) facilitating study of envelope functions in the higher solution bands, where approximation methods fail and simulations become difficult. In particular, we are interested in the effect of drift spaces and asymmetry on the remarkable second-band beam compression effect previously reported for the FD case [2].

Instead of solving the envelope equations directly, as we did in Ref. [2], we use here the linear single-particle equations and the phase-amplitude method to get the exact envelope functions and phase advances. To indicate briefly that, in our model, the periodic lattice of quadrupole doublets has piecewise-constant focusing but may have unequal gap lengths, we introduce the abbreviation *FoDO*.

## FOCUSING MODEL

We assume a focusing function  $\kappa(z)$  that is periodic over a lattice with period  $2L$ , so that  $\kappa(z + 2L) = \kappa(z)$ . We take  $\kappa(z)$  to be piecewise constant with value  $+\kappa_{\max}$  in the focus and  $-\kappa_{\max}$  in the defocus sections, which have equal length. For convenience throughout, we define

$$k \equiv \sqrt{\kappa_{\max}}. \quad (1)$$

Our FoDO model is then described for the  $xz$ -plane by Eqs. (2) and Fig. 1:

$$\kappa(z) \equiv \begin{cases} +k^2, & 0 < z < \eta L; \\ 0, & \eta L < z < \eta L + d_1; \\ -k^2, & \eta L + d_1 < z < 2\eta L + d_1; \\ 0, & 2L - d_2 < z < 2L. \end{cases} \quad (2)$$

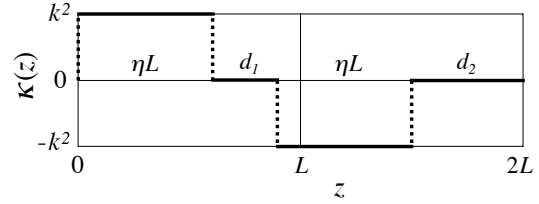


Figure 1: Model for  $xz$ -plane in one cell of a periodic FoDO lattice. The quadrupoles have equal lengths  $\eta L$ ; gap lengths are  $d_1$  and  $d_2$ . The cell starts at  $z = 0$  with  $\kappa > 0$  (focus). The  $yz$ -plane field map is the same but inverted.

Since the FoDO lattice cell (Fig. 1) has equal focus and defocus lengths, the fields have antisymmetry about each gap center. For a matched beam, this yields a relationship between the envelopes  $a(z)$  and  $b(z)$  in the  $xz$  and  $yz$  planes, respectively. One finds that

$$b(z) = a(2z_c - z), \quad (3)$$

where  $z_c$  is the center of any gap. Therefore, we only need to analyze  $a(z)$  in what follows.

## DEFINITIONS

We define the *gap asymmetry parameter*

$$\mu \equiv \frac{d_2 - d_1}{2d}, \quad (4)$$

where

$$d \equiv \frac{d_2 + d_1}{2} = (1 - \eta)L \quad (5)$$

so that

$$d_1 = d(1 - \mu), \quad d_2 = d(1 + \mu). \quad (6)$$

\* Supported in part by the U.S. Department of Energy under Contract No. DE-AC02-05CH11231.  
Prepared in part by LLNL under Contract DE-AC52-07NA27344.

The *normalized gap lengths* are

$$\nu \equiv kd = k(1 - \eta)L = \frac{1 - \eta}{\eta} \varphi, \quad (7)$$

$$\nu_1 \equiv kd_1 = \nu(1 - \mu), \quad (8)$$

$$\nu_2 \equiv kd_2 = \nu(1 + \mu). \quad (9)$$

The *focusing strength parameter*, used throughout this paper, is defined by

$$\varphi \equiv \eta kL. \quad (10)$$

We introduce the following quantities that depend on this parameter:

$$\begin{aligned} sn &\equiv \sin \varphi, & cs &\equiv \cos \varphi, \\ sh &\equiv \sinh \varphi, & ch &\equiv \cosh \varphi. \end{aligned} \quad (11)$$

In the limit  $\eta \rightarrow 1$ ,  $sn$ ,  $cs$ ,  $sh$ , and  $ch$  become identical with the functions defined in Ref. [2].

## MATCHED BEAM ENVELOPES

For a beam with emittance  $\epsilon$ , negligible space charge, and arbitrary periodic focus function  $f(z)$ , the  $xz$ -plane envelope function  $a(z)$  is determined by [5]:

$$a(z)'' + f(z)a - \frac{\epsilon^2}{a^3} = 0 \quad (12)$$

along with initial or periodic conditions for  $x$  and  $y$ . We assume  $\epsilon_x = \epsilon_y = \epsilon$ . Without space charge, the beam distribution may be KV or a class of physically realistic distributions.

For a matched beam without space charge, it is unnecessary to solve the nonlinear equation (12) directly. Instead, we find the envelopes [6] using the phase-amplitude method [1], [4], which yields the result

$$\frac{1}{\epsilon} a^2(z) = \frac{\mathbf{M}_{12}(z)}{\mathbf{P} \sqrt{1 - (\frac{1}{2} \text{Tr } \mathbf{M})^2}}, \quad (13)$$

with

$$\mathbf{P}(\varphi) \equiv \text{sign}(\sin \varphi). \quad (14)$$

The function  $\mathbf{P}$  provides the correct sign for the radical for any phase advance [2].

The matrix  $\mathbf{M}$  is obtained by multiplying the transfer matrices for the segments of a lattice cell. In the case of a FoDO cell, these segments—taken in the order of Fig. 1—have transfer matrices [1], [7]

$$\mathbf{M}_F = \begin{pmatrix} cs & \frac{1}{k} sn \\ -k sn & cs \end{pmatrix}, \quad \mathbf{M}_{O_1} = \begin{pmatrix} 1 & d_1 \\ 0 & 1 \end{pmatrix},$$

$$\mathbf{M}_D = \begin{pmatrix} ch & \frac{1}{k} sh \\ k sh & ch \end{pmatrix}, \quad \mathbf{M}_{O_2} = \begin{pmatrix} 1 & d_2 \\ 0 & 1 \end{pmatrix}.$$

The matrix for the entire cell, starting at  $z = 0$  in Fig. 1, is

$$\mathbf{M}(0) = \mathbf{M}(2L) = \mathbf{M}_{O_2} \mathbf{M}_D \mathbf{M}_{O_1} \mathbf{M}_F. \quad (15)$$

The ranges of  $z$  for the four individual segments are indicated in Fig. 1, namely,  $\eta L$ ,  $d_1$ ,  $\eta L$ , and  $d_2$ . If  $z \neq 0$  but, for example,  $z$  lies within the first segment, then  $\eta L$  and  $\mathbf{M}_F$  split into ranges  $z$  and  $\eta L - z$  as seen in Eq. (20).

## Stability and Phase Advance $\sigma$

A single-particle orbit is stable if  $2 \cos \sigma = |\text{Tr } \mathbf{M}| < 2$  [1]. We calculate the trace from  $\mathbf{M}(0) = \mathbf{M}_{\text{III}} \mathbf{M}_F$  where

$$\mathbf{M}_{\text{III}} \equiv \mathbf{M}_{O_2} \mathbf{M}_D \mathbf{M}_{O_1} = \begin{pmatrix} A_1 & \frac{2B+sh}{k} \\ k sh & A_2 \end{pmatrix}, \quad (16)$$

$$A_1 \equiv ch + \nu_2 sh, \quad A_2 \equiv ch + \nu_1 sh, \quad (17)$$

$$B \equiv \nu ch + \frac{1 - \mu^2}{2} \nu^2 sh. \quad (18)$$

Then

$$\cos \sigma = \frac{\mathbf{M}_{11} + \mathbf{M}_{22}}{2} = (ch + \nu sh)cs - B sn \quad (19)$$

gives the phase advance, which agrees with the result given by Lund and Bukh [3]. The envelope solution will be stable for all values of  $\varphi$  for which the right-hand side of Eq. (19) lies within the range  $[-1, 1]$ . Such regions of  $\varphi$  or  $kL$  are referred to as pass bands. Reference [2] shows how these bands are related to the branches of  $\cos \sigma$ .

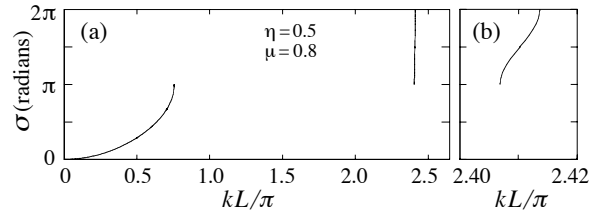


Figure 2: (a) Phase advance from Eq. (19) for the first two stable bands. (b) Band 2 with the  $kL$  axis magnified.

## Exact Matched Beam Envelopes

For an arbitrary point  $z$  in the first (focus) segment, the transfer matrix is obtained from  $\mathbf{M}_{\text{III}}$  after pre- and post-multiplying by the two subunits of  $\mathbf{M}_F$  referred to above.

$$\begin{aligned} \mathbf{M}^f(z) &= \begin{pmatrix} \cos kz & \frac{1}{k} \sin kz \\ -k \sin kz & \cos kz \end{pmatrix} \mathbf{M}_{\text{III}} \times \\ &\quad \begin{pmatrix} \cos k(\eta L - z) & \frac{1}{k} \sin k(\eta L - z) \\ -k \sin k(\eta L - z) & \cos k(\eta L - z) \end{pmatrix}. \end{aligned} \quad (20)$$

The superscript “f” means that  $z$  is restricted here to the focusing segment. We define  $F(\varphi, z) \equiv k \mathbf{M}_{12}^f$  and find, with Eqs. (13) and (19), the exact focus-segment envelope:

$$a^2(\varphi, z) = \epsilon \eta L \frac{F(\varphi, z)}{\mathbf{P} \varphi \sqrt{1 - (\frac{1}{2} \text{Tr } \mathbf{M})^2}} \quad (21)$$

$$\begin{aligned} F(\varphi, z) &= (ch + \nu sh)sn + \mu \nu sh \sin[\varphi(1 - 2z/\eta L)] \\ &\quad + B cs + (B + sh) \cos[\varphi(1 - 2z/\eta L)]. \end{aligned} \quad (22)$$

There is no space here to present the exact solutions for all four segments—see Ref. [6]. Instead, we show the result for a complete cell graphically in Figs. 3 and 4. The lattice

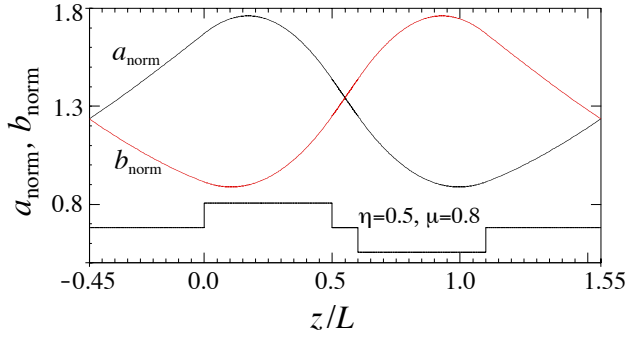


Figure 3: Envelope  $a_{\text{norm}} \equiv a(z)/\sqrt{\epsilon L}$  from Eq. (21) and Ref. [6]. Focus parameter  $kL = 0.60565\pi$  gives  $\sigma = 80^\circ$ .

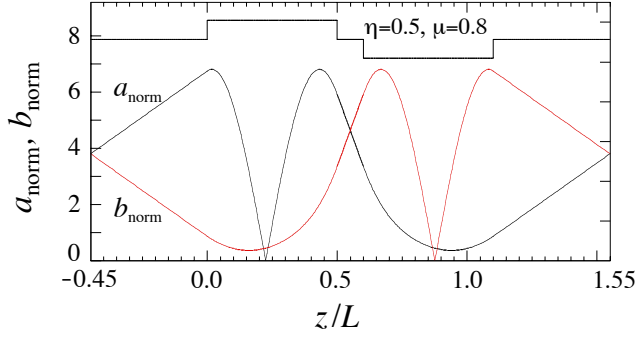


Figure 4: Same as Fig. 3 but with focus parameter  $kL = 2.41027\pi$ ;  $\sigma = 270^\circ$ , the middle of the second pass band.

parameters are  $\eta = 0.5$ ,  $\mu = 0.8$ , with phase advances  $\sigma = 80^\circ$  and  $\sigma = 270^\circ$ , respectively. Figure 3 uses the same parameters as in a numerical example by Lund et al. [4]. Our first-band envelopes are very like theirs (which include some space charge), but somewhat more compressed.

In the figures,  $a(z)$  was obtained from our exact results, while  $b(z)$  simply used Eq. (3). The origin has been shifted from that in Fig. 1. It is placed at the center of the second drift space in order to display the matched-beam symmetry described earlier.

### Other Topics: peak excursion, beam compression

The peak value of the envelope determines whether the beam can pass through a given channel. There is an optimum value of the focus strength for each pass band, as seen in Fig. 5.

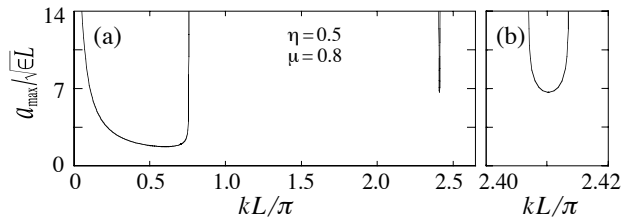


Figure 5: Peak envelope values taken from Ref. [6]. Same  $\eta$  and  $\mu$  as in Figs. 2, 3, and 4. (a) First two stable bands. (b) Second band magnified.

Beam compression in even bands is due to envelope minima in the  $xz$  and  $yz$  planes occurring at or near the same  $z$ . Ref. [2] shows that the effect becomes extreme near the outer band edge (but it notes that caveats apply). The effect is even larger when there are drift spaces because the focusing strength must be increased. For  $\eta = 0.5$ ,  $\mu = 0.0$ , and  $\sigma = 356.75$ , the area compression ratio is  $1.17 \times 10^6$ . However, if the asymmetry parameter  $\mu$  is finite, the  $xz$  and  $yz$  compression points become separated and, for  $\mu = 0.8$  (Fig. 6), the area compression ratio is only  $7 \times 10^4$ .

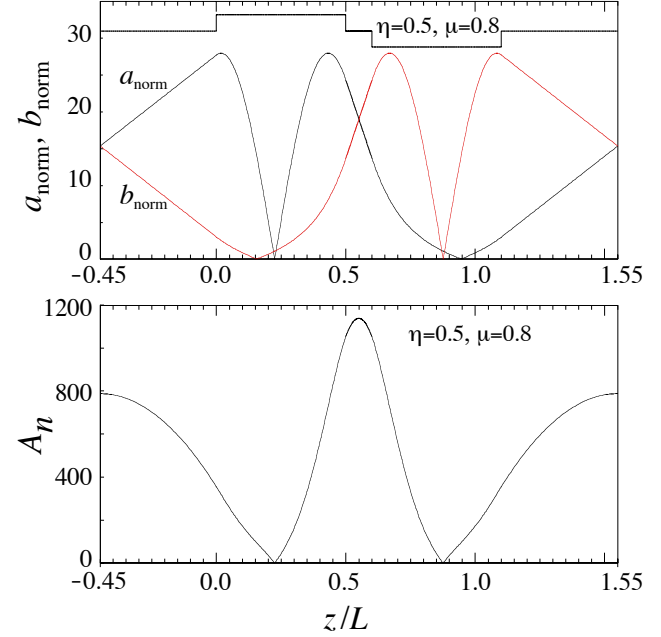


Figure 6: Normalized  $a(z)$ ,  $b(z)$ , and  $A_n(z) \equiv \pi ab$  near outer edge of band 2:  $kL = 2.41361\pi$ ;  $\sigma = 356.6^\circ$ . The beam compression ( $7 \times 10^4$ ) is reduced because the gaps have unequal length and the  $a(z)$  and  $b(z)$  minima do not coincide—see text.

## ACKNOWLEDGMENTS

We thank S.M. Lund and E.P. Lee for suggesting the transfer matrix method of solution.

## REFERENCES

- [1] E. D. Courant and H. S. Snyder, *Ann. of Phys.* **3**, 1 (1958).
- [2] O. A. Anderson and L. L. LoDestro, *Phys. Rev. ST Accel. Beams* **12** (2009).
- [3] S. M. Lund and B. Bukh, *Phys. Rev. ST Accel. Beams* **7**, 024801 (2004).
- [4] S. M. Lund, S. H. Chilton, and E. P. Lee, *Phys. Rev. ST Accel. Beams* **9**, 064201 (2006).
- [5] I. M. Kapchinskij and V. V. Vladimirovskij, in *Conf. on High Energy Accel. and Instrum.* (CERN Sci. Inf. Service, Geneva, 1959), p. 274.
- [6] O. A. Anderson and L. L. LoDestro, *Tech. Rep. LBNL-1812E*, Lawrence Berkeley Laboratory (2009).
- [7] M. Reiser, *Particle Accelerators* **8**, 167 (1978).